Experimental and Theoretical Study of Excited-State Structure and Relaxation Processes of Betaine-30 and of Pyridinium Model Compounds

V. Kharlanov and W. Rettig*

Institute of Chemistry, Humboldt University of Berlin, Brook-Taylor-Strasse 2, D-12489 Berlin, Germany

Received: May 15, 2009; Revised Manuscript Received: August 12, 2009

The long-wavelength absorption band of 2,6-diphenyl-4-(2,4,6-triphenylpyridinium-1-yl) phenolate (betaine-30, **B30**) in ethanol and 1-chlorobutane shifts to the blue by cooling in the temperature range of 294−128 K. In addition, **B30** shows fluorescence in both solvents at 77 K, which is absent at room temperature. The study of the ground and excited state of **B30** and its model compound 4-(pyridinium-1-yl)-phenolate **PyPo** by DFT/TDDFT calculations indicates that for the perpendicular conformation, the ground state possesses a charge-separated closed-shell hole pair (hp) electronic configuration, and the S_1 state corresponds to a biradicaloid electronic structure (dd) with a small dipole moment caused by an unpaired electron on each of the orthogonal fragments. Following the absorption process, there is a driving force for geometrical relaxation within the S_1 state toward an orthogonal arrangement of the phenolate and the pyridinium ring. In this final S_1 equilibrium geometry, the energy gap between the excited and the ground state is strongly reduced and causes very efficient radiationless deactivation of the S_1 state at room temperature. At 77 K, the viscous barrier hindering large-amplitude motion enables the appearance of the fluorescence from the partially or nonrelaxed excited Franck−Condon structure. By variation of the donor and acceptor strength of the two moieties, the energy gap for perpendicular systems can be tuned, allowing, in principle, the switching between the two cases hp < dd and hp > dd. This enables a new access to the efficient construction of mnemonic systems and NLO dyes.

1. Introduction

2,6-Diphenyl-4-(2,4,6-triphenylpyridinium-1-yl)-phenolate, or simply pyridinium *N*-phenolate (betaine-30, **B30**), is a well-known strongly solvatochromic dye. Its long-wavelength absorption band is shifted from λ_{max}= 810 nm in diphenylether to 453 nm in water.[1−9] This large blue shift in polar solvents is explained by the strong dipole moment change in the $S_0 \rightarrow S_1^{FC}$ transition responsible for the absorption band. The experimental dipole moments of **B30** are 14.8 (from dielectric constant measurements) and 6.2 D (from solvatochromic shifts) for ground and excited states, respectively.[2,10,11] Femtosecond transient absorption results[9] indicate a substantial contribution of intramolecular motion in the relaxation of the excited state.

Quantum chemical calculations correlate well with the experimental results. The calculated ground-state dipole moment μ_g of **B30** in the gas phase is in the range of 12.9−16.8 D.[12−18] The S_1^{FC} dipole moment μ_e is 3.9 D according to INDO/CI calculations.[13] These values were determined for the ground-state equilibrium geometries of **B30** in the gas phase. The torsion angles of the phenyl substituents at positions 2 and 6 of the heterocyclic ring (Scheme 1) are 52−55°, and the angle between the planes of the phenolate and the pyridinium ring is 60−68° (AM1 and HF/3-21G.[12−18]). The geometrical characteristics of the calculated structures are in good agreement with X-ray data. The corresponding twist angles in a crystal of a **B30** analogue containing a bromine atom in the para position of the 4-phenyl group are very similar to the calculated results of **B30**, with one significant difference[19a] regarding the torsion of the phenyl group in position 4. This torsion angle is only 18°, in contrast to the calculated value of 37−45° for the betaine **B30** without the bromine atom. This difference could be due to crystal packing effects or the electronic influence of the bromine atom. The characteristics calculated for **B30** refer to only one of many possible conformers differing by the combination of the phenyl torsion angles. A recent X-ray analysis of a **B30** model compound **PyPo** (see Scheme 1) indicated a twist angle of 47° between the two rings.[19b]

On the other hand, the dipole moments and the transition energies of a further conformer calculated by AM1 and INDO/CI[14] differ only weakly from the values indicated above, although the torsion angles of the phenyl groups attached to the phenolate fragment are somewhat changed. Only a few conformations were studied, however, and a conformational analysis was not performed. In this situation, it is impossible to relate the calculated characteristics to the conformer of the global minimum. In order to gain more information about the

SCHEME 1: Investigated Compounds

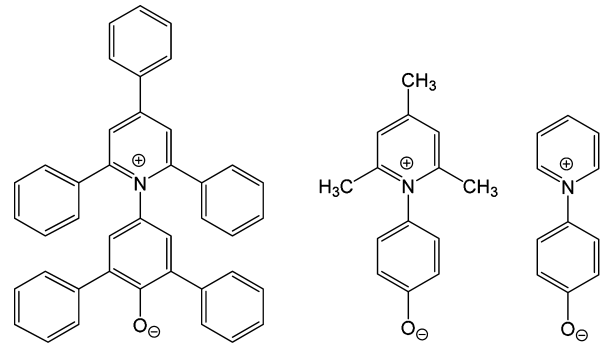

B30 **PyPo_3m** **PyPo**

* To whom correspondence should be addressed.

10.1021/jp904537k CCC: $40.75
Published on Web 09/11/2009

importance of conformational effects, we calculated the properties of two optimized conformers of **B30** which differ in the arrangement of the phenyl groups in position 4 of the pyridinium ring.

Studies of the **B30** vis absorption dependence on the temperature showed a red shift with heating of the solution.[6−8] The absorption maximum was shifted from $\lambda_{max} = 492$ to 520 nm in methanol, from 543 to 564 nm in ethanol, and from 619 to 637 nm in acetonitrile in the range of 280−343 K. The thermochromic behavior of **B30** is interpreted as the result of decreasing solvent polarity with increasing temperature.[6] The authors assumed also that **B30** in alcohols exists in two conformers because of the observation of an isosbestic point for the spectra at different temperatures. One species is thought to be free **B30**, and the other is thought to be a complex of **B30** with a solvent molecule.

The small excited-state dipole moment is caused by the charge transfer from the phenolate to the pyridinium ring in the $S_0 \rightarrow S_1^{FC}$ transition according to INDO/CI calculations.[13,14] The nature and characteristics of other transitions were not determined.

AM1 calculations including a self-consistent reaction field SCRF showed that the solvent influence on **B30** is very weak regarding the equilibrium geometry of the phenyl substituents. The interplanar angles of these phenyl groups decrease by only 2.0−2.5° compared to those in the gas phase for a series of solvents of different polarity.[14]

The ground-state dipole moment in acetonitrile (19 or 25 D[15]) is significantly larger than the gas-phase dipole moment (13 D[14]), consistent with a large molecular polarizability. The calculations showed also a very good agreement of the transition energy values with experimental data in different solvents.[14]

Three relaxation processes are assumed in the excited state of **B30**. The first one is a large-amplitude intramolecular rearrangement.[9,13,16] INDO/CI calculations for different torsion angles of the phenolate ring in the S_1 state suggest that an orthogonal structure is reached in the gas phase because the S_1^{FC} energy decreases by rotation of the phenolate ring to the 90° twisted geometry.[13] Analogous results follow from PPP excited-state calculations.[16] The second process is an intramolecular electron transfer (ET)[20−27] with a characteristic time in the range of 0.09−0.90 ps for different solvents.[9] The third process is return to the ground state by back electron transfer (bET).[9] It is also suggested that for the last process, vibrational levels of the ground state are involved.[25] The rate of the bET process is slower than that of ET, with characteristic times in different solvents at room temperature being 2−12 ps[9,20−27] according to transient absorption experiments.

These extremely fast processes cause the absence of steady-state fluorescence; the fluorescence of **B30** at room temperature has never been observed. The fluorescence (stimulated emission) is also not observed in picosecond transient absorption experiments.[20−24] The stimulated emission at room temperature was observed only in subpicosecond transient absorption experiments (in the time interval of 80−800 fs after excitation).[9] The fluorescence quenching can be explained by a very rapid (subps) change of the nature of the S_1 state. The nature of this conversion process is unknown.

Resonance Raman profiles for the vibrational modes of **B30** were used in studies focusing on the determination of the solvent reorganization energy in the excited state. The determination is based on a time-dependent theory and a Brownian oscillator model.[7,8,28,29]

The simplest betaine model compound 4-(pyridinium-1-yl) phenolate **PyPo** possesses a twisted ground-state structure with a torsion angle between the fragments of 25−41° in the gas phase[30−34] according to different calculations (AM1, HF/6-31G(d), MP2/6-31G(d), DFT, CASSCF). The ground-state torsion angle increases in polar solvents (from 39.9° in the gas phase to 45.6° in acetonitrile and 46.8° in water).[30] Direct excited-state geometry optimization of **PyPo** by CIS/6-31G(d) supports the formation of a perpendicular structure in the S_1 state. These calculations also showed that the nitrogen atom prefers a pyramidal sp^3 hybridized geometry after electron transfer. The authors suggest a $\pi\pi^*$ nature of the absorption transition because the LUMO orbital is delocalized over both rings in the Franck−Condon geometry.

In the present contribution, we want to report new absorption and fluorescence measurement results for **B30**. These results are interpreted by quantum chemical modeling of **B30** and the closely related model compounds **PyPo_3m** and **PyPo** (Scheme 1) by both semiempirical and ab initio calculations. In the case of the model betaine **PyPo**, the S_1 state and its relaxation pathway were also studied.

2. Experiment and Calculations

2.1. Materials. The betaine **B30** was received from Fluka and used as supplied.

The solvents were of spectroscopic quality (ethanol, methanol and acetonitrile) and for liquid chromatography (1-chlorobutane). For reasons discussed below, triethylamine was added to the solutions in a few cases, and no spectral changes were observed.

2.2. Apparatus and Methods. The vis absorption spectra at room temperature were recorded with an ATI Unicam UV2 spectrophotometer (U.K.). Low-temperature absorption measurements were carried out by a UV−vis spectrophotometer UV mini 1240 Shimadzu in which an Oxford Instruments cryostat was mounted for the cooling of a 1 × 1 cm quartz cuvette.

Corrected fluorescence and uncorrected fluorescence excitation spectra at 77 K were measured in a quartz tube with 5 mm diameter using an SLM AMINCO AB2 fluorimeter fitted with a Dewar vessel with a quartz window. The optical density of the solutions at room temperature was 0.8−1.2 when measured in a 1.0 cm cuvette. The glass-state formation was verified by the transparency of the solution and by the surface distortion within the tube. The attempt to detect fluorescence at room temperature was carried out without success using a much larger absorbance of the solutions.

2.3. Calculations. All calculations used the Gaussian 03[35] and Turbomole 5.7[36] suite of programs. The ground-state studies were carried out by the Hartree−Fock HF method as well as by HF with MP2 correlation correction and by the density functional theory (DFT) using Becke's three-parameter hybrid method and the correlation functional of Lee, Yang, and Parr (LYP) with the correlation potentials VWM(III) (for calculations with Gaussian 03) and VWM(V) (for the calculations with Turbomole). In order to distinguish between these calculation procedures, the Gaussian 03 calculations are termed B3LYP_g and the Turbomole ones B3LYP_tm. For the ground state, identical results were found.

The excited states were calculated by HF with single configuration interaction (CIS) of 20 occupied and 20 unoccupied orbitals (CI = 20/20) within Gaussian as well as by time-dependent density functional theory TDDFT with the B3LYP hybrid method within Turbomole. In contrast to Gaussian 03, Turbomole is able to optimize excited states by TDDFT. A full geometry optimization of the ground-state (**B30** and the model betaines) and excited-state potential minima (for the model

TABLE 1: Long-Wavelength Absorption Band (λ_{max}, nm) of B30, Measured in Different Solvents at Room Temperature and Comparison to a Gas Phase-Calculation (ZINDO/s for the AM1 equilibrium geometry, $\alpha_{eq} = 56°$)

solvent	B30	B30[a]
C_6H_5Cl		777
n-BuCl	768	
DMSO	632	634
CH_3CN	617	627
EtOH	551[b]	551
MeOH	512[c]	516
ZINDO/s	898 ($f = 0.33$)	

[a] From ref 2. [b] In EtOH with triethylamine. [c] In MeOH with triethylamine.

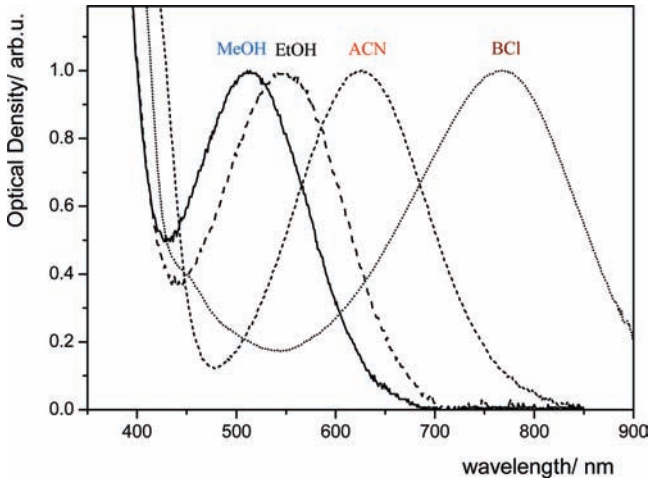

Figure 1. Normalized absorption spectra of **B30**, measured in different solvents at room temperature, methanol (MeOH), ethanol (EtOH), acetonitrile (ACN), and 1-chlorobutane (BCl).

betaines only) was performed and controlled by vibrational analysis (Hessian matrix) comparing different basis sets indicated in the Results and Discussion section.

Given the large number of atoms, **B30** was also optimized in the ground state using the semiempirical AM1 method. In this case, the absorption transitions were calculated by ZINDO/s for the AM1-optimized equilibrium geometry of the compounds. Both calculations were performed using the Gaussian 03 package.

3. Results and Discussion

3.1. Low-Temperature Absorption Spectra of B30. The position of the long-wavelength absorption band of **B30** at room temperature depends strongly on the solvent polarity (Table 1, Figure 1). There was no difference in the absorption spectrum of **B30** dissolved in pure alcohols (methanol and ethanol) and that in the same alcohols with addition of the base triethylamine, indicating that there is no protonation of the betaine in these solvents. Fast cooling to 77 K of **B30** dissolved in alcohols (MeOH, EtOH) causes a shift of the absorption band to shorter wavelengths, and the color of the solution changes from violet (room temperature) to orange (glassy state), consistent with the strongly blue-shifted fluorescence excitation spectrum at 77 K (see below) as compared to the room-temperature absorption.

The absorption spectrum measured in ethanol at variable temperatures within the temperature range of 294−128 K (Figure 2a) shows a blue shift of the long-wavelength band of $\Delta\lambda = 65$ nm from $\lambda_{max} = 552$ to 487 nm induced by the cooling. This shift is accompanied by an absorption band intensity

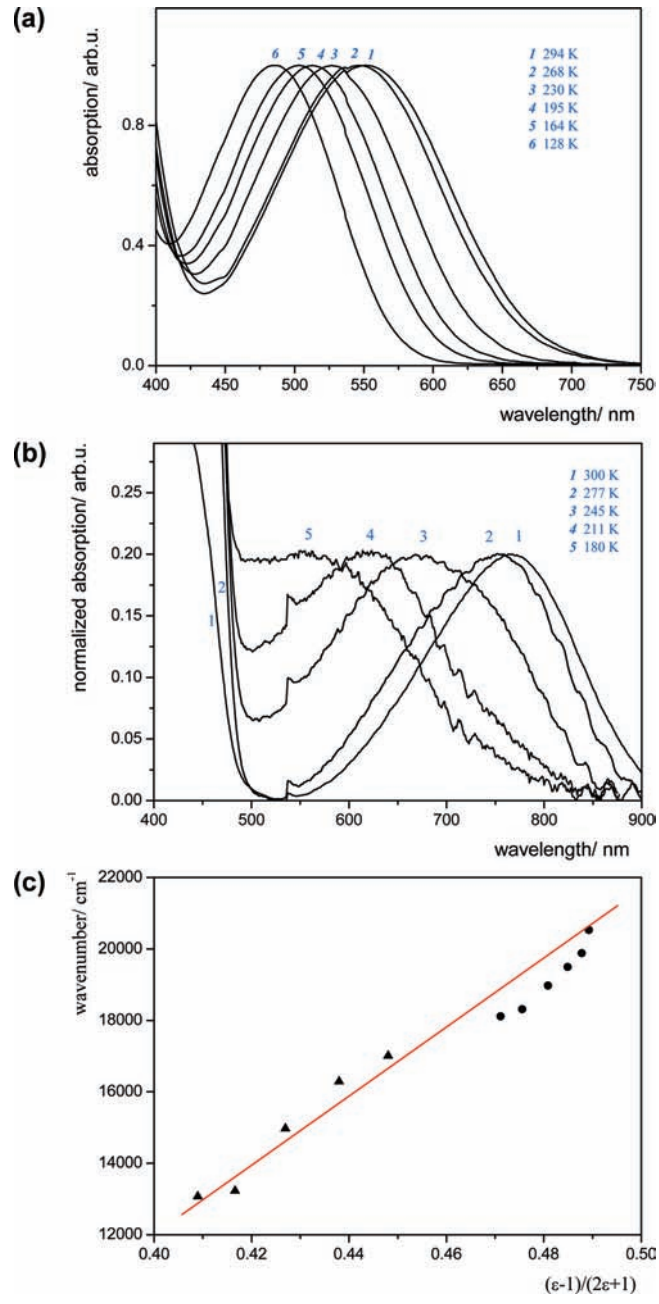

Figure 2. (a) Temperature dependence of the normalized absorption spectrum for **B30**, measured in ethanol between 128 and 294 K. (b) Temperature dependence of the normalized absorption spectrum for **B30**, measured in 1-chlorobutane between 180 and 300 K. (c) Long-wavelength absorption band maxima for **B30**, measured in ethanol (circles) and 1-chlorobutane (triangles) in dependence of the polarity function $f(\varepsilon) = (\varepsilon - 1)/(2\varepsilon + 1)$ at different temperatures. The straight line is a linear least-squares fit of all data points.

increase by a factor of around 1.8. A similar shift is also observed in 1-chlorobutane (Figure 2b), where the absorption band shifts by $\Delta\lambda = 227$ nm from $\lambda_{max} = 768$ to 540 nm after cooling from 300 to 148 K.

The hypsochromic shift of the absorption band with lowering of the solution temperature can be explained by a concomitant increase of the solvent polarity[30,37−44] because the dielectric constant of the solvents rises upon cooling down to the freezing point. The dependence of the absorption band maximum on the solvent polarity function $f(\varepsilon) = (\varepsilon - 1)/(2\varepsilon + 1)$ is displayed as a function of temperature in Figure 2c; $f(\varepsilon)$ was determined

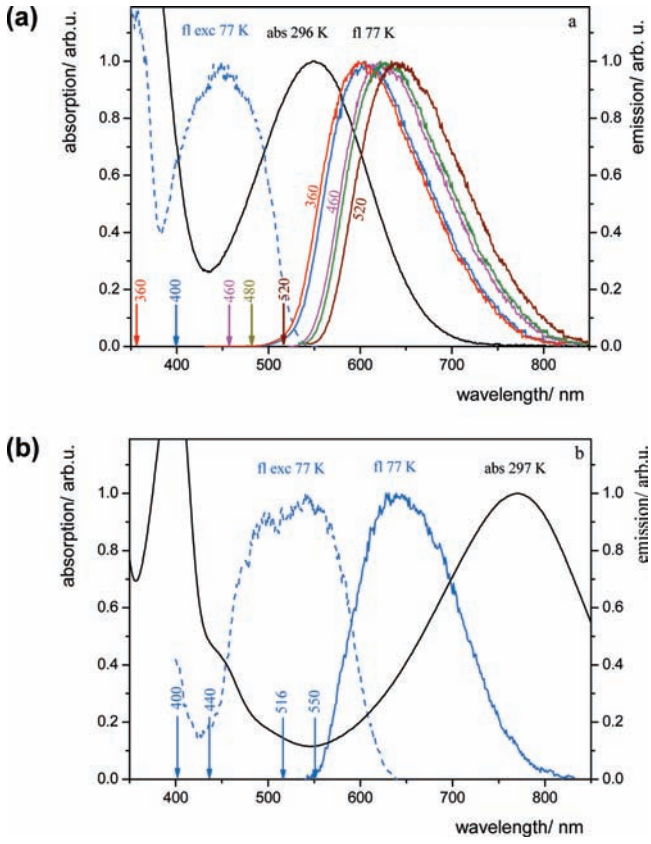

Figure 3. Normalized absorption (at 296 K), corrected fluorescence (at 77 K), and uncorrected fluorescence excitation (at 77 K) spectra of **B30**, measured in ethanol with triethylamine (a) and in 1-chlorobutane (BuCl) (b). The arrows indicate the fluorescence excitation wavelength. For BuCl, the fluorescence spectrum is independent of the excitation wavelength.

from the known data of the dielectric constant ε at different temperatures (for ethanol[38,41] and 1-chlorobutane[40]).

3.2. Fluorescence of B30 at 77 K. Fluorescence of solutions of **B30** at room temperature could not be detected, neither in pure alcohols nor in alcohols with added triethylamine (TEA). Fluorescence is also absent in other solvents at room temperature (toluene, $CHCl_3$, CH_3CN, DMSO), consistent with a very fast deactivation of the S_1 state.

However, fluorescence could be detected for solutions of **B30** in ethanol at 77 K (Figure 3). The fluorescence maximum is situated at around $\lambda^{fl}_{max} \simeq 600$ nm and is shifted moderately for different excitation wavelengths. Excitation at 360, 404, 460, 480, and 520 nm results in fluorescence spectra with maxima at 604, 606, 622, 626, and 634 nm, respectively. This excitation wavelength dependence indicates a weak inhomogeneous broadening of the emission caused by different absorption centers, possibly solute−solvent arrangements or conformers. The emission properties of **B30** are independent of the addition of TEA to the solution.

The uncorrected fluorescence excitation spectrum of **B30** in ethanol at 77 K is strongly blue shifted in comparison to the absorption spectrum at room temperature (Figure 3).

Fluorescence of **B30** is also observed in 1-chlorobutane at 77 K (Figure 3) with a band maximum at around 640 nm, which does not change for the different excitation wavelengths used. It is red shifted by only $\Delta\nu = 2510$ cm^{-1} relative to the fluorescence excitation maximum at 77 K but blue shifted by $\Delta\nu = 5550$ cm^{-1} as compared to the absorption band maximum at room temperature.

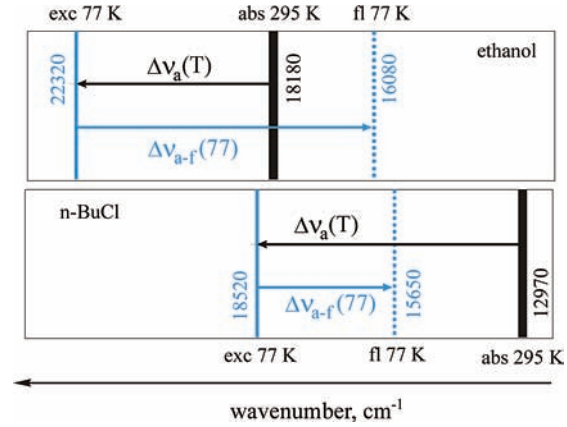

Figure 4. Position of the absorption band at room temperature (bold solid lines), as well as fluorescence (dashed lines) and fluorescence excitation (thin solid lines) at 77 K for **B30**, measured in ethanol and 1-chlorobutane.

The fluorescence energies as well as the shift of absorption and excitation spectra are summarized in Figure 4. It can be seen that the Stokes shift for ethanol at 77 K is larger than that for 1-chlorobutane, such that the fluorescence in 1-chlorobutane at 77 K remains blue shifted with respect to the absorption spectrum at room temperature, in contrast to ethanol (Figure 4). This might be connected with the fact that ethanol possesses a residual flexibility even at 77 K, whereas 1-chlorobutane may resist more strongly to any driving forces for large-amplitude geometrical relaxations. The blue shift of the excitation spectra induced by temperature lowering is rather similar for both solvents. This is consistent with the linear behavior of the absorption blue shift shown in Figure 2c.

The presence of fluorescence of solutions of **B30** at 77 K can be explained with a slowing down of the S_1 state deactivation rate as compared to that at room temperature. It is possible that the decreased rate is induced by the high viscosity of the solvents, connected with the hindering of large-amplitude relaxation motions leading toward the quenching geometrical structure.

3.5. Calculation of Ground- and Excited-State Properties of B30. Our investigation focuses on two possible conformers of **B30** which differ in the torsion angle of the phenyl group in position 4 of the pyridinium ring relative to the torsional angles of the other phenyl groups. The optimized geometry of the two conformers was independent of the starting geometry.

The equilibrium geometry of conformer **B30_a** in the ground state was calculated by AM1 and by DFT (B3LYP/cc-pVDZ). The DFT optimized equilibrium geometry (Figure 5) is characterized by strongly twisted phenyl rings in positions 2 and 6 (around 54.0°) and a weaker twist for the ring in position 4 (29.3°) of the pyridinium moiety. The torsion angle to the phenolate ring is 55°. The phenyl rings on the phenolate ring moiety are twisted by ∼34°. The torsion angles of the phenyls in positions 2 and 6 calculated with AM1 are quite similar to those obtained by the ab initio calculations (around 54°). Other twist angles are also similar, for example, the twist angle for the phenolate fragment (49°) and the 4-phenyl substituent on pyridinium (31°). All calculated data correlate with the previously published ones.[12−18]

The geometry of the second conformer **B30_b** (see Figure 5, right-hand side) is very similar to the first one, except that the phenyl in position 4 is twisted by 31.5° in the opposite direction as compared to **B30_a** (Figure 5). The conformer **B30_a** is more stable by 0.34 kcal/mol (B3LYP).

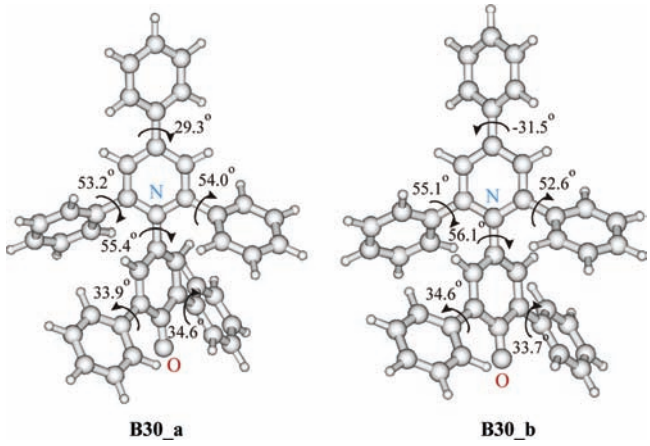

Figure 5. The S_0 state optimized equilibrium geometries for the two conformers **B30_a** and **B30_b** (left and right, respectively) (B3LYP/cc-pVDZ). The main difference is the relative orientation of the phenyl ring in position 4 of the pyridinium ring (the torsion angles are 29.3 and −31.5°). The conformer **B30_a** is significantly more stable than **B30_b** (by 0.34 kcal/mol).

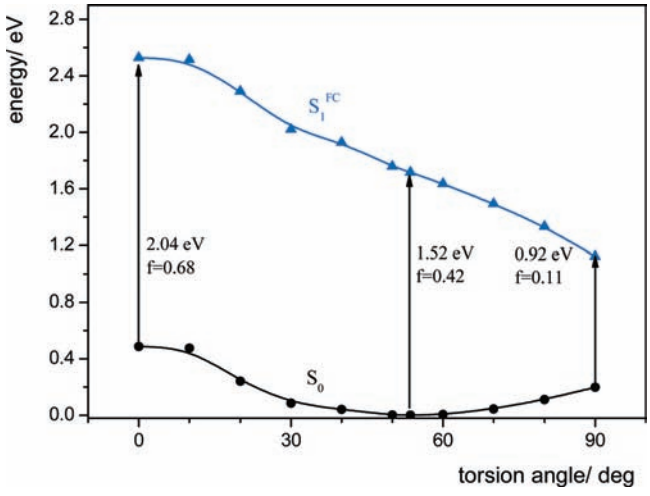

Figure 6. The S_0 and S_1^{FC} potentials of betaine **B30_b** calculated by TDDFT/cc-pVDZ (for S_1) and B3LYP/cc-pVDZ (for S_0). The S_1^{FC} potentials were calculated for the optimized ground-state geometry for rigid twist angles between the phenolate and the pyridinium ring.

According to the B3LYP calculations of **B30_b** in the gas phase, the rotation of the phenolate ring from the equilibrium geometry (56.1°) to the planar and orthogonal geometries in S_0 corresponds to saddle points of first order signifying an activation barrier for rotation of 11.2 and 4.6 kcal/mol, respectively (Figure 6).

According to CIS/cc-pVDZ calculations (Table 2), the nature of the low-energy transition of **B30_a** and **B30_b** for the equilibrium geometries is an electron density redistribution from the phenolate moiety including the phenyl rings toward the pyridinium ring including the 4-phenyl substituent. As the orbitals are delocalized (nonperpendicular geometry), the transition is allowed for both conformers, but the transition energies differ significantly (1.76 and 1.52 eV for **B30_a** and **B30_b**, respectively), possibly due to the different relative conformation of the phenyl ring in the 4 position of the pyridinium ring. This strong difference in absorption may be one cause for the inhomogeneous broadening of the fluorescence at 77 K. The charge-transfer nature of the $S_0 \rightarrow S_1$ transition is connected with strong but similar dipole moment changes from 12.1 and 12.3 D to 0.60 and 0.50 D for **B30_a** and **B30_b**, respectively.

The electronic nature of the forbidden $S_0 \rightarrow S_2$ transition (the oscillator strength is 0.01 for both conformers) is connected with a shift of electron density from the lone pair of the oxygen atom to the π^* orbital of the heterocyclic ring ($n\pi^*$ transition), resulting in a large dipole moment of the S_2 state (15.3 D for **B30_a** and 11.7 D for **B30_b**). The strongly polar $n\pi^*$ state is consistent with the localized nature of the $n\pi^*$ transition. The $n\pi^*$ transition energies for the conformers differ very weakly (1.97 eV for **B30_a** and 1.95 eV for **B30_b**); see also Table 2.

The $S_0 \rightarrow S_3$ transition possesses also CT nature. However, in contrast to the $S_0 \rightarrow S_1$ transition, the charge is redistributed from a delocalized orbital (phenolate with pyridinium) to a more localized one (the pyridinium with the phenyl groups in the 2 and 6 positions). The transition is characterized by a strong dipole moment change. The S_3 state dipole moment is 5.26 (**B30_a**) and 0.61 D (**B30_b**), in contrast to the large ground-state dipole moment of 12.1 (**B30_a**) and 12.3 D (**B30_b**) (Table 2).

The Franck−Condon $S_0 \rightarrow S_1$ potential calculated for the ground-state optimized geometry of **B30_b** with a fixed pyridinium−phenolate interplanar angle shows that the energy decreases with rotation of the phenolate fragment from the planar to the 90° twisted structure (Figure 6). The S_0 orthogonal structure possesses a larger dipole moment (14.7 D) than the ground-state equilibrium structure at 56.1°. The S_1^{FC} state of the perpendicular structure possesses a small dipole moment of 0.85 D. The energy gap between the excited and the ground state is only 0.92 eV at 90°. An unpaired electron is approximately located on the pyridinium ring (total charge of the ring is −0.16) and on the phenolate (total charge is +0.03) (not taking into account the charges on the pendant phenyl groups). This indicates a biradicaloid nature of this state with a small difference of total charge on the submoieties.

3.6. Ground-State Study of the Sterically Hindered Trimethyl-Substituted Model Compound PyPo_3m. In the model compound **PyPo_3m**, the methyl substituents at positions 2 and 6 of the pyridinium moiety cause an even stronger sterical interaction than the phenyl groups in **B30**. The angle between the phenolate and the pyridinium rings is calculated to be 63° for **PyPo_3m** in the gas phase (Figure 7). The bond lengths and bond angles of the aromatic rings of the betaine model are similar to those of **B30**. However, the replacement of the three 2,4,6-phenyl groups by methyl in the model compound causes a change of the nature of the $S_0 \rightarrow S_1$ transition. For this partially twisted geometry, the low-energy allowed transition at 2.02 eV is of $n\pi^*$ character with a significant admixture of $\pi\pi^*$ according to the TDDFT results. Some electron density is shifted from the lone pair of oxygen to a π^* orbital delocalized over both aromatic rings. Correspondingly, the dipole moment of the S_1 state (11.3 D) differs only weakly from the ground-state dipole moment (14.4 D) (Table 2).

The allowed $S_0 \rightarrow S_2$ transition ($f = 0.22$) is of slightly higher energy (2.05 eV) and is of CT character (Table 2).

The $S_0 \rightarrow S_3$ transition has also CT nature. However, the charge shift from the phenolate to the pyridinium ring is smaller than that for the $S_0 \rightarrow S_2$ transition, and the dipole moment of the S_3 state is larger (5.22 D, Table 3).

3.7. Ground- and Excited-State Property of the Sterically Unhindered Model Betaine PyPo. The simplest model betaine **PyPo** is more planar in the ground state than **PyPo_3m**, as expected. The absence of the methyl groups in the 2 and 6 positions of the pyridinium ring of **PyPo** causes a torsion angle

TABLE 2: Characteristics [ΔE transition energy in eV, oscillator strength f, $\mu(S_0)$ and $\mu(S_i)$ dipole moments of the S_0 and S_i states, and transition nature] of the Absorption Transitions $S_0 \rightarrow S_i$, Calculated for the S_0 State Equilibrium Geometry of the Conformers B30_a and B30_b and for the Model Betaine PyPo_3m in the Gas Phase

transition	characteristic of transition	**B30_a**[a] TD_g/cc-pVDZ ($\alpha = 55.4°$)	**B30_b**[a] TD_g/cc-pVDZ ($\alpha = 56.1°$)	**PyPo_3m**[b] TD_g/aug-cc-pVDZ ($\alpha = 62.6°$)
$S_0 \rightarrow S_1$	ΔE eV, $(f) - \lambda$, nm	1.76 (0.45)−706	1.52 (0.42)−723	2.02 (0.03)−615
	$\mu(S_0) \rightarrow \mu(S_1)$, D	12.1 → 0.60	12.3 → 0.50	14.4 → 11.3
	nature	$\pi\pi^*$ **CT**[c]	$\pi\pi^*$ **CT**[c]	$n\pi^* + \pi\pi^*$[f]
$S_0 \rightarrow S_2$	ΔE eV, $(f) - \lambda$, nm	1.97 (0.01)−629	1.95 (0.01)−635	2.05 (0.22)−605
	$\mu(S_0) \rightarrow \mu(S_2)$, D	12.1 → 15.3	12.3 → 11.7	14.4 → 0.57
	nature	$n\pi^*$[d]	$n\pi^*$[d]	$\pi\pi^* + n\pi^*$ **CT**[g]
$S_0 \rightarrow S_3$	ΔE eV, $(f) - \lambda$, nm	2.00 (0.03)−620	1.99 (0.03)−624	2.18 (0.02)−568
	$\mu(S_0) \rightarrow \mu(S_3)$, D	12.1 → 5.26	12.3 → 0.61	14.4 → 5.22
	nature	$\pi\pi^*$ **CT**[e]	$\pi\pi^*$ **CT**[e]	$\pi\pi^*$ **CT**[h]

[a] For the S_0 state equilibrium geometry optimized by B3LYP_g/cc-pVDZ. [b] For the S_0 state equilibrium geometry optimized by B3LYP_g/aug-cc-pVDZ. [c] The $\pi\pi^*$ transition (charge transfer from a delocalized orbital including the phenolate fragment and the pyridinium ring to a π orbital on the pyridinium ring including the phenyl group in position 4). [d] The $n\pi^*$ transition (with charge transfer from the lone pair on the oxygen to a delocalized π orbital). [e] The $\pi\pi^*$ transition (charge transfer from a delocalized orbital including the phenolate fragment and the pyridinium ring to an orbital localized on the pyridinium ring and the two phenyl groups in positions 2 and 6). [f] The $n\pi^*$transition (transition from the lone pair on oxygen to a delocalized π orbital with some admixture of a $\pi\pi^*$ transition). [g] The $\pi\pi^*$transition with some admixture of $n\pi^*$. [h] Charge transfer from the phenolate fragment to the pyridinium ring.

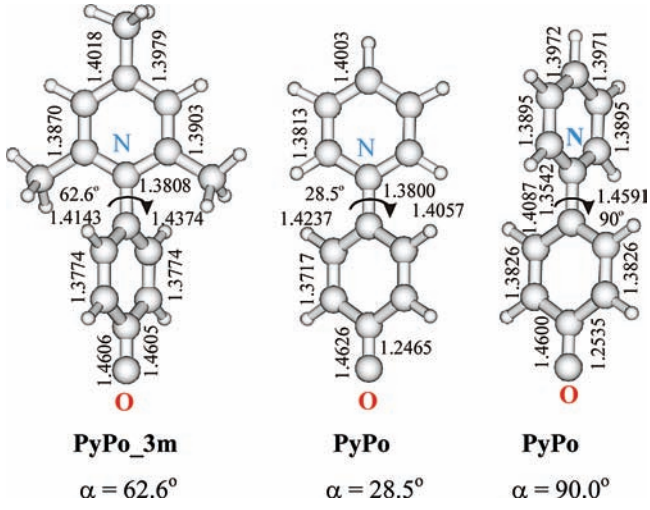

Figure 7. The S_0 state optimized geometries, calculated by B3LYP/aug-cc-pVDZ, of the model betaines **PyPo_3m** (equilibrium twist angle $\alpha = 62.6°$) and **PyPo** ($\alpha = 28.5°$) and **PyPo** in the transition-state structure ($\alpha = 90.0°$).

TABLE 3: Characteristics [ΔE transition energy, eV, oscillator strength f, $\mu(S_0)$ and $\mu(S_i)$ dipole moments of the S_0 and S_i states, and their transition nature] of the Absorption Transitions $S_0 \rightarrow S_i$, Calculated for the S_0 State with Optimized Equilibrium and Orthogonal Geometries (B3LYP_tm/aug-cc-pVDZ) of the Model Compound PyPo in the Gas Phase

		PyPo	
transition	characteristic of transition	TDDFT_tm/aug-cc-pVDZ ($\alpha = 28.5°$)	TDDFT_tm/aug-cc-pVDZ ($\alpha = 90.0°$)
$S_0 \rightarrow S_1$	ΔE eV, $(f) - \lambda$, nm	2.23 (0.02)−556	0.01 (0.00)−20677
	$\mu(S_0) \rightarrow \mu(S_1)$, D	11.2 → 4.77	17.4 → 1.15
	nature	$n\pi^* + \pi\pi^*$ **CT**[a]	$\pi\pi^*$ **CT**
$S_0 \rightarrow S_2$	ΔE eV, $(f) - \lambda$, nm	2.48 (0.50)−499	0.74 (0.00)−1682
	$\mu(S_0) \rightarrow \mu(S_2)$, D	11.2 → 10.2	17.4 → 0.45
	nature	$\pi\pi^*$[c]	$n\pi^*$ **CT**
$S_0 \rightarrow S_3$	ΔE eV, $(f) - \lambda$, nm	2.52 (∼0.00)−492	0.88 (0.00)−1410
	$\mu(S_0) \rightarrow \mu(S_3)$, D	11.2 → 6.33	17.4 → 2.24
	nature	$\pi\pi^*$ **CT**[b]	$\pi\pi^*$ **CT**

[a] The $n\pi^*$transition with an admixture of $\pi\pi^*$ (charge transfer from the phenolate fragment to the pyridinium ring). [b] Charge transfer from the phenolate fragment to the pyridinium ring. [c] Delocalized orbitals.

of only 28.5° and a short distance of 140.57 pm between the rings, in contrast to 62.6° and 143.74 pm for **PyPo_3m** (Figure 7). The short bond and the small twist angle are consistent with a considerably stronger mesomeric interaction between the two rings. The trend for planarity of **PyPo** is also demonstrated by the small activation energy for rotation to 0° (1.19 kcal/mol), whereas the rotation to 90° increases the energy by 12.6 kcal/mol (B3LYP/aug-cc-pVDZ) (Figure 8).

The Franck−Condon $S_0 \rightarrow S_1$ transition for the fully optimized equilibrium geometry (B3LYP/aug-cc-pVDZ) possesses a relatively large energy (2.23 eV) and is weakly allowed ($f = 0.04$) (Table 3). This transition is of $n\pi^*$ nature with some admixture of $\pi\pi^*$ and is connected with a charge transfer from the phenolate to the heterocyclic ring. The dipole moment of the S_1 state is reduced to 4.8 D, in contrast to 11.2 D for S_0.

The strongly allowed $S_0 \rightarrow S_2$ transition of $\pi\pi^*$ nature has an energy of 2.48 eV and is connected with a very small dipole moment change with respect to the ground state ($\mu_e = 10.2$ D; see Table 3).

The 90° orthogonal geometry of the S_0 state of **PyPo** differs from the equilibrium one regarding the bond lengths (Figure 7). The most significant change is in the bond connecting pyridinium and phenolate rings, which lengthens from 138 to 146 pm (Figure 7) due to the breakage of the mesomeric interaction. The CN bond of the pyridinium ring decreases to 135 pm as compared with 138 pm. Other distances within the rings differ little. The electronic structure is characterized by a full localization of the negative charge on the phenolate and the positive one on the pyridinium ring. This electron distribution results in a very large dipole moment of 17.4 D for S_0 (Table 3). Most significantly, the S_1 Franck−Condon state of the 90° twisted geometry is characterized by a very small energy gap between the ground and excited states (only 0.01 eV) and a much lower dipole moment (1.15 D) than that for the ground-state equilibrium geometry, caused by a near-complete electron transfer from the donor fragment of the betaine to the acceptor one. The S_1 state therefore possesses one unpaired electron on each ring and is therefore of biradicaloid nature. The energy difference from the ground state to other excited states is also small (0.74 and 0.88 eV for S_2 and S_3). The nature of these states is also charge transfer, as indicated by the small value of

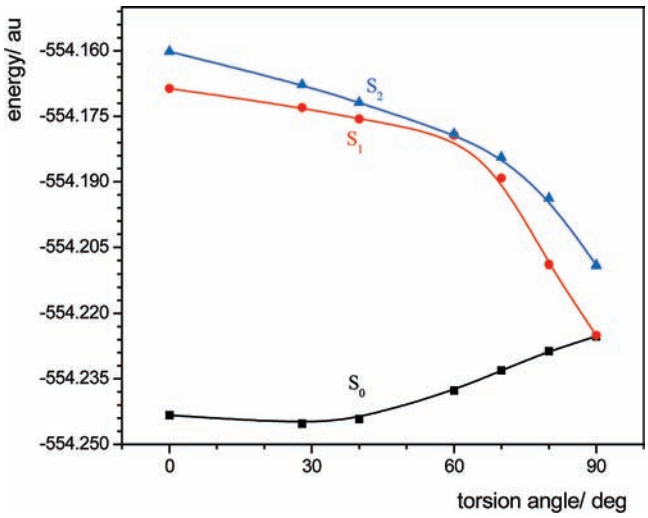

Figure 8. The S_0, S_1, and S_2 state potentials of model betaine **PyPo** calculated by TDDFT/aug-cc-pVDZ (for S_1 and S_2) and B3LYP/aug-cc-pVDZ (for S_0). Except for 90°, the potentials of the ground and excited states were determined by full optimization for the torsion angle between the phenolate and the pyridinium rings, both kept fixed with the constraint of C_2 or C_{2v} symmetry.

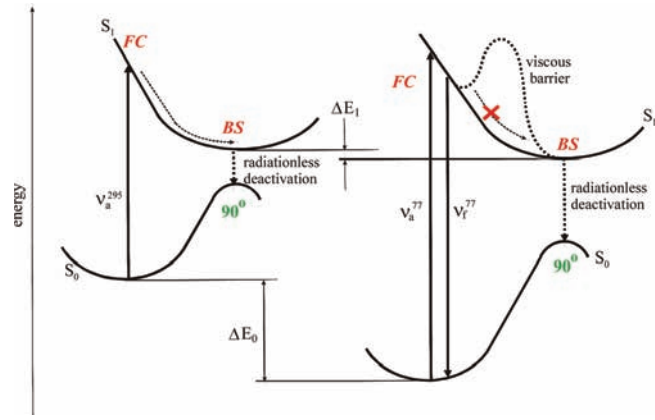

Figure 9. Qualitative scheme of the excited-state processes of **B30** at room (left) and low temperatures (77 K) (right). The large viscous barrier at 77 K stops the angular relaxation in S_1 toward a highly twisted geometry with a small energy gap. For 77 K, the increased solvent polarity leads to stabilizations ΔE_0 (strongly polar ground state) and ΔE_1 (weakly polar excited state), which is larger in the ground than in the excited state due to the difference in dipole moments.

the dipole moment (0.45 D for S_2 and 2.24 D for S_3). All transitions are forbidden.

The energies of the S_1 and S_2 states decrease with twisting of the fragments from the planar to the orthogonal geometry (Figure 8). The fully optimized planar structure of S_1 (within C_{2v} symmetry constraints) is of nπ* nature and is characterized by a large dipole moment (11.5 D), which is only a little smaller than that of the ground state (12.1 D). The properties at 0 and 90° are therefore very different. In contrast to the small energy gap and large dipole moment change for the Franck−Condon transition at 90°, the dipole moment change is small and the energy gap large for 0°. The geometry optimization of the 90° twisted structure of S_1 (within C_2 symmetry constraints) could not be performed by TDDFT calculations because of calculational instabilities at this geometry. With the rigid optimized ground-state geometry at 90°, the energy of the "FC S_1 state" is above that of the closed-shell ground state.

The trend of the potential energy changes clearly demonstrates that the S_0 and S_1 states approach each other upon twisting and come very close, with the S_1 state going energetically downhill and the S_0 state uphill.

3.8. Excited-State Processes of B30. The experimental and theoretical results obtained in the present work suggest a qualitative scheme for the excited-state processes of **B30** (Figure 9). The excitation at room temperature and at 77 K from the ground-state equilibrium betaine structure creates a low-polarity Franck−Condon **FC** state which relaxes to the S_1 state with orthogonal arrangement of the pyridinium and phenolate rings in low-viscosity media. This structure of biradicaloid nature (**BS**) with unpaired electrons located in the 90° twisted fragments possesses a small dipole moment and a small S_1-S_0 energy gap. The formation of the biradicaloid structure **BS** of **B30** by angular relaxation causes efficient radiationless deactivation of the S_1 state and is similar to the behavior of related biphenyl-type systems which possess large energy gaps at the ground-state equilibrium geometry but small S_1-S_0 gaps for the twisted geometry. As shown in section 3.9, this is a general phenomenon encompassing both betaines and twisted intramolecular charge transfer (TICT) systems (for reviews, see refs 45 and 46). The nonradiative S_1-S_0 transition results in the formation of the high-polarity betaine structure in the ground state as the result of a back electron transfer from the pyridinium to the phenolate ring. For sufficiently narrow energy gaps at 90°, as found for **B30** and its model compounds, this leads to complete fluorescence quenching because at room temperature, the formation of **BS** occurs very efficiently as the surrounding medium allows for ultrafast relaxation processes. At 77 K in the glass state, the medium creates a viscous barrier to large-amplitude motions, and the formation of **BS** is less efficient. This allows fluorescence to be emitted from quasi-stable structures with the geometry near **FC** (see Figure 9).

Such intrinsic viscous barriers hindering large-amplitude intramolecular motion at low temperature were previously considered also for other molecules.[47−50]

3.9. Decoupled Biphenyl-Type Molecules: A Blueprint for Optimized NLO and Mnemonic Devices. The model calculations shown above indicate a general trend for **B30** and its derivatives.

(i) The ground and excited states can come very close energetically, consistent with an absorption spectrum in the infrared.

(ii) The closest approach occurs generally for the decoupled 90° geometry.

(iii) At the same time, the dipole moment of the CT state increases with twisting and reaches a maximum for 90°.

(iv) The polar solvent interaction changes the ground-state equilibrium geometry toward stronger solute−solvent interaction, that is, in highly polar solvents, the geometry approaches the decoupled case at 90°.

(v) For the donor−acceptor combinations investigated here, the energy gap corresponding to the relaxed excited-state geometry is very small and can be expected to strongly enhance nonradiative excited-state decay, explaining the absence of fluorescence at room temperature.

Fabian and Zahradnik[51] have shown that orbital decoupling leading to CT systems is a general way of producing systems with small energy gaps, that is, absorbing in the NIR region. This can be achieved by modulating the electron donor−acceptor properties of the subgroups and at the same time maintaining the decoupling between them. Possible ways for decoupling are twisting, as shown here, but also possible are T-shaped arrangements or donor−bridge−acceptor systems with electronically

insulating bridges. A further possibility is juxtaposition of the two moieties. This approach is used by nature in the photosynthetic reaction center.[52]

For a certain combination of donor and acceptor, the S_0 and S_1 surfaces will touch at 90°. This is a general phenomenon which can occur for systems with a charge-separated ground state but also for systems where the charge-separated state is an excited one. There are many experimental studies for the latter case. The properties mentioned in points (i)−(iv) then apply to the excited state, where the system relaxes to the perpendicular geometry. Such systems belong to the class of TICT states.[45,46] In the case of TICT states with the representative system 4-(dimethylamino)benzonitrile (DMABN), highly solvatochromic CT fluorescence is observed, indicating that this state is very polar and that, unlike for the system **B30**, the S_1-S_0 energy gap is sizable. Michl and Bonačić−Koutecký[53,54] showed that this charge separation and relaxation to the perpendicular geometry is much more general and can also occur if external charges are applied. The donor−acceptor modulation is not only possible by replacement of the submoieties, but also, the influence of an electric field can lead to the degeneracy of the ground and excited states at 90° or generally for a decoupled geometry, at least judging from quantum chemical calculations. Early calculations have been performed for various twist angles of symmetric ethylene in the neighborhood of a point charge.[53,55] Recently, a related biaromatic model system has been studied using high-level CASSCF calculations, and it could be shown that surface crossing through a conical intersection can occur even if ground- and excited-state minima are separated by a small but nonzero energy gap through the involvement of a second, the so-called aromatization, coordinate.[56]

This principle can be applied to many biphenyl-type molecules for generating a new class of nonlinear optical materials. The synthesis of molecular systems with near-perpendicular aromatic six-membered rings was already achieved, and their donor−acceptor properties were varied, which resulted in changes of the physical properties (absorption energy, linear and nonlinear polarizabilities).[57,58] We will show here that a general theoretical correlation method can be used for predicting near-surface touching. This method can consequently be used for the tailor-making of dyes with desired properties, for example, regarding absorption energy and NLO properties.

If we consider 90° twisted biaromatic systems, the energy difference between the charge-separated and the nonpolar excited state is related to the energy difference between the donor and acceptor orbital relevant to the CT transition. For the zero-coupling case and the prototype molecules, the highest molecular orbital is normally localized on the donor, HOMO(D), and the lowest unoccupied orbital is on the acceptor, LUMO(A). In this case, if for the S_1 state the HOMO to LUMO configuration has a large weight, the absorption energy ΔE_{01} is given approximately by the energy difference between these two orbitals $\Delta\varepsilon_{HL}$ (Figure 10a), plus a simple correction due to the electron−electron interaction (Coulomb and exchange integrals[53]).

For a certain combination of $\Delta\varepsilon_{HL}$ and Coulomb/exchange integrals, their contribution cancels, and ΔE_{01} becomes zero. This is the "critically heterosymmetric" case.[53] The two states which are degenerate here are the dot−dot (dd) state, corresponding to the occupancy of HOMO(D) and LUMO(A) with one electron, and the hole pair (hp) state (two paired electrons in one orbital)[46,53−55] (Figure 10b). The dd state can be of polar or nonpolar nature, depending on the nuclear charges, with the example ethylene/aminoborane being the simplest case;[53] see also Figure 10a for the example of betaines. If we designate the nonpolar state as N and the polar one as Z (for zwitterionic) we can call these two cases "type I" (hp is N and dd is Z) and "type II" (hp is Z and dd is N; Figure 10c). We immediately realize that the usual case of TICT systems belongs to type I, whereas **B30** and related compounds belong to type II, but the intrinsic CT mechanism is the same.

For a sufficiently large $\Delta\varepsilon_{HL}$ and the zero-coupling case, the dd state will be S_1 and the ground state hp. This corresponds to the situation in **B30** and in the usual TICT molecules. However, if we increase the donor strength, raising the energy of HOMO(D), or if we increase the acceptor strength, lowering the energy of LUMO(A), or for both changes simultaneously, we will arrive at the critically heterosymmetric situation and even get beyond it, with dd below hp. This corresponds to a biradicaloid ground state with either polar (type I) or nonpolar properties (type II); see Figure 10c.

Crossing the critically heterosymmetric case provides the key for generating NLO materials of unprecedented hyperpolarizabilities,[57] but it can also be used for constructing materials showing "mnemonic effects".[45]

The hyperpolarizability β is connected with ΔE_{01} and with the dipole moment change $\Delta\mu_{01}$ between the ground and excited states by eq 1, where μ_{01} is the transition dipole moment between these two states.[57] If the energy gap ΔE_{01} between the two states is small and can be tuned and $\Delta\mu_{01}$ is large, the molecular hyperpolarizability β can become very large, leading to efficient NLO materials. The only hindrance for efficiency is the transition moment μ_{01}, which is zero for pure CT transitions in completely decoupled systems. Some trade-off in terms of a weak coupling, that is, deviation from 90°, is therefore necessary.

$$\beta \propto \Delta\mu_{01}(\mu_{01})^2/(\Delta E_{01})^2 \qquad (1)$$

Mnemonic systems were first discussed by Stolarczyk and Piela.[59] They were later reviewed in the context of TICT systems.[45] Basically, a system with a polar S_1 state (N below Z) can be switched to a situation where Z is below N by creating chains of (DA) pairs and/or by applying an appropriate very strong electric field. The action of this field can be described by inspection of Figure 10c by an effective change of the DA strength (horizontal axis) leading to a passage through the conical intersection. By inverting the field, the crossing is also possible in the opposite direction. Molecules like **B30** with Z-type ground states can favorably be used for this switching by applying a field which destabilizes the polar S_0(Z) state. It can be expected that the properties of materials containing such dyes will change drastically by switching from a polar to a nonpolar ground state. In principle, such a switching can be used for constructing information-storing devices, wherefrom the name "mnemonic systems" is derived. It has to be remarked, however, that in order to arrive at a macroscopical switching effect, sufficiently decoupled donor and acceptor moieties are necessary (e.g., through twisting by steric interaction), and the DA system needs to have a specific orientation with respect to the electric field vector, that is, macroscopic molecular orientation is necessary.

In order to show an example for a crossing of the critically heterosymmetric point by "chemical means", we use the **B30**

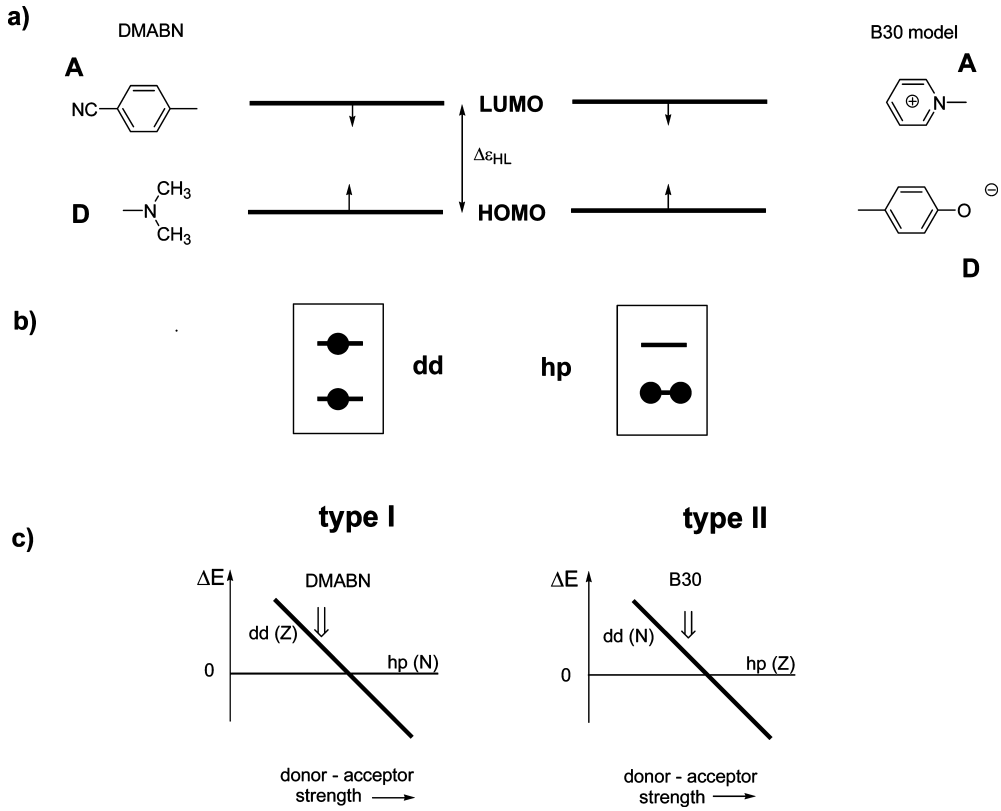

Figure 10. (a) Examples for two classes of molecules with a lowest dd or hp state. These possess different CT properties due to the replacement of an atom on the donor D and on the acceptor A by elements in adjacent columns of the periodic system. In the prototype decoupled TICT system (90° twisted **DMABN**, left, type I), the hp state is weakly polar, but in **B30** and model compounds, (the prototype betaine molecules, right, type II), it is highly polar because the core charge is increased and decreased by one unit in both D (amino N in **DMABN** to oxygen in B30) and A (carbon cyano group in **DMABN** to nitrogen in **B30**). These different classes can be distinguished as type I (polar dd state) and type II (polar hp state) systems. The arrows mark the energetic influence of increasing the donor and acceptor strength on the orbital energies. (b) Definition of the hole pair (hp, two spin-paired electrons in the highest occupied molecular orbital) and the dot−dot (dd) state (two electrons in two different orbitals localized on D and A). If the HOMO−LUMO energy gap is sufficiently large and the HOMO is localized on D and the LUMO on A, the dd state is of higher energy than the hp state. Increasing the donor and/or acceptor strength (corresponding to the arrows in a) leads to a lowering of the dd state relative to the hp state. For sufficiently strong DA combinations and for complete orbital decoupling, the dd state is situated below the hp state. (c) Influence of DA variations on the energy difference ΔE between the dd and the hp states. The hp state is arbitrarily fixed to zero. At the crossing of the two lines, the critically heterosymmetric situation is reached, corresponding to a conical intersection. If the complete orbital decoupling is lifted, for example, by twisting away from 90°, the degeneracy is lifted; this also occurs by changing the donor and/or acceptor strength. Instead of changing the donor and acceptor strength by chemical means (substituents), the conical intersection can also be reached by applying an electric field. To the left of the conical intersection (crossing of the two lines), the CT state of type I systems is S_1 and is zwitterionic (Z) and of dd nature. It needs to be stabilized by the field. For type II systems, the Z state is S_0 and of hp nature and needs to be destabilized. To the right of the conical intersection, reversal of the electric field induces the approach to the conical intersection. In both these cases, the absorption energy will be shifted to the red by applying the field.

model compound **PyPo** and compare it to derivatives with changes of donor/and or acceptor (Table 4). We expect that a weakening of D as in **3** and **4** raises the dd state with respect to the hp state. The linkage of the donor to the pyridinium ring in position 4 instead of position 1 (**PyPo**) creates a stronger acceptor with a reduced orbital energy gap $\Delta\varepsilon_{HL}$. Correspondingly, the dd state is now situated below the hp one, with a clear reversal of the two types of states. This situation is summarized in Figure 11.

Higher-level ab initio calculations of Ratner[57,58] and Isborn[60] support our results and confirm that the energy of the non-charge-separated biradicaloid state (dd) is situated below the zwitterionic state (hp) for the orthogonal structure of **1** at least for the gas phase. Consistent results were also obtained for **4** by Haas et al.,[56] that is, dd and hp states are very close-lying for 90° twist. These authors found that their energetic order can be reversed by solvent polarity and by the "aromatization coordinate", that is, bond length changes within the benzene ring.

4. Conclusion

Our spectroscopic experiments with **B30** showed several new properties of this betaine. Low-temperature absorption in a single solvent leads to blue shifts, consistent with room-temperature absorption in differently polar solvents. The analysis of this temperature dependence indicates that it is due to an increase of the solvent dielectric constant at low temperature. The blue shift observed upon cooling is linearly connected with the change of the solvent polarity function $f(\varepsilon) = (\varepsilon - 1)/(2\varepsilon + 1)$. Whereas at room temperature any fluorescence was absent, we could detect fluorescence at 77 K. Together with the theoretical results obtained, this indicates a large-amplitude twisting motion as the cause for the fluorescence quenching.

The ab initio study of the S_1 state of **B30** and the model compound **PyPo** showed that there is a driving force in S_1 leading toward an orthogonal conformation with a very small

TABLE 4: Properties of Orthogonal Biaromatic Systems with Different Donor−Acceptor Properties, Calculated by B3LYP/aug-cc-pVDZ (S_0 state optimization) and TDDFT ($S_0 \rightarrow S_1$ transition energy for the B3LYP with optimized 90° twisted geometry, CI = 20/20) for the Systems

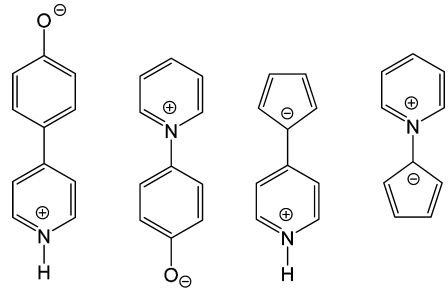

1 **2** **3** **4**

PyPo

	$\Delta\varepsilon_{HL}$,[a] eV	$\Delta E(S_0 \rightarrow S_1)$, eV	S_0	S_1
1	−0.15	−0.56	dd	hp
2	−0.69	0.01	hp	dd
3	−0.91	0.13	hp	dd
4	−1.45	0.70	hp	dd

[a] $\Delta\varepsilon_{HL} = \varepsilon_H - \varepsilon_L$.

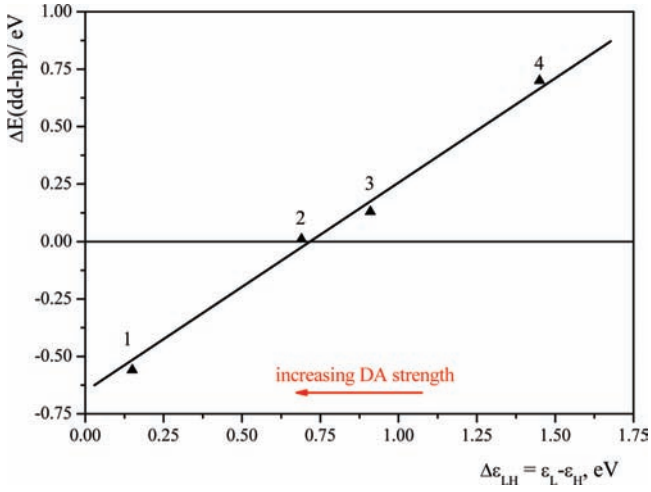

Figure 11. Calculated energy difference ΔE(dd−hp) between the dot−dot and the hole pair state for perpendicular type II compounds (Franck−Condon TDDFT/aug-ccpVDZ calculations). For compound **4**, the normal situation arises, (polar hp is the ground state), whereas in **1**, a reversed situation (dd is below hp) is calculated (for experimental systems, deviations from 90° may cause a mixing between these two states). Molecules **2** and **3** are predicted to be good candidates for mnemonic switching due to their very small energy gap between dd and hp states. The structures of **1**−**4** are given in Table 4.

S_1-S_0 energy gap and biradicaloid properties, which are responsible for the fast nonradiative relaxation at this geometry.

These systems, when rigidly kept in their orthogonal conformation, are, in principle, capable of electric-field-induced state switching and of unprecedented NLO performance. A simple procedure is shown to qualitatively predict favorable systems for these properties.

Acknowledgment. Financial support by the Deutsche Forschungsgemeinschaft (SFB 448) and help by Dr. W. Weigel with the low-temperature absorption experiments is gratefully acknowledged.

References and Notes

(1) Reichardt, C. *Solvents and Solvent Effects in Organic Chemistry*,3rd ed.; Wiley-VCH: Weinheim, Germany, 2003; Chapter 6.2, p 330ff and Chapter 7, p 389ff.
(2) (a) Reichardt, C. *Chem. Rev.* **1994**, *94*, 2319. (b) Reichardt, C. *Pure Appl. Chem.* **2008**, *80*, 1415.
(3) (a) Reichardt, C. *Angew. Chem.* **1979**, *91*, 119. (b) Reichardt, C. *Angew. Chem., Int. Ed. Engl.* **1979**, *18*, 98.
(4) Reichardt, C.; Röchling, A.; Schäfer, G. *J. Phys. Org. Chem.* **2003**, *16*, 682.
(5) Dimroth, K.; Reichardt, C.; Siepmann, T.; Bohlmann, F. *Liebigs Ann. Chem.* **1963**, *661*, 1.
(6) Dimroth, K.; Reichardt, C. *Justus Liebigs Ann. Chem.* **1969**, *727*, 93.
(7) Reichardt, C. *Justus Liebigs Ann. Chem.* **1971**, *752*, 64.
(8) Zhao, X.; Burt, J. A.; McHale, J. L. *J. Chem. Phys.* **2004**, *121*, 11195.
(9) Kovalenko, S. A.; Eilers-König, N.; Senyushkina, T. A.; Ernsting, N. P. *J. Phys. Chem. A* **2001**, *105*, 4834.
(10) (a) Liptay, W. *Angew. Chem.* **1969**, *81*, 195. (b) Liptay, W. *Angew. Chem., Int. Ed. Engl.* **1969**, *8*, 177.
(11) Liptay, W.; Dumbacher, B.; Weisenberger, H. *Z. Naturforsch., A: Phys. Chem.* **1968**, *23a*, 1613.
(12) Bartkowiak, W.; Lipinski, J. *J. Phys. Chem. A* **1998**, *102*, 5236.
(13) Mente, S. R.; Maroncelli, M. *J. Phys. Chem.* **1999**, *103*, 7704.
(14) DeAlencastro, R. B.; Neto, J. D. M.; Zerner, M. C. *Int. J. Quantum Chem.* **1994**, *28*, 361.
(15) Lobaugh, J.; Rossky, P. J. *J. Phys. Chem. A* **2000**, *104*, 899.
(16) Lobaugh, J.; Rossky, P. J. *J. Phys. Chem. A* **1999**, *103*, 9432.
(17) Hogiu, S.; Dreyer, J.; Pfeiffer, M.; Brzezinka, K.-W.; Werncke, W. *J. Raman Spectrosc.* **2000**, *31*, 797.
(18) Lipinski, J.; Bartkowiak, W. *J. Phys. Chem. A* **1997**, *101*, 2159.
(19) (a) Allmann, R. *Z. Kristallogr.* **1969**, *128*, 115. (b) Wojtas, L.; Pawlica, D.; Stadnicka, K. *J. Mol. Struct.* **2006**, *785*, 14.
(20) Reid, P. J.; Barbara, P. F. *J. Phys. Chem.* **1995**, *99*, 3554.
(21) Levinger, N. E.; Johnson, A. E.; Walker, G. C.; Barbara, P. F. *Chem. Phys. Lett.* **1992**, *196*, 159.
(22) Levinger, N. E.; Johnson, A. E.; Walker, G. C.; Barbara, P. F. *Chem. Phys. Lett.* **1992**, *196*, 159.
(23) Akesson, E.; Johnson, A. E.; Levinger, N. E.; Walker, G. C.; Dubruil, T. P.; Barbara, P. F. *J. Phys. Chem.* **1992**, *96*, 7859.
(24) Reid, P. J.; Simson, A.; Jarzela, W.; Schlief, R. E.; Johnson, A. E.; Barbara, P. F. *Chem. Phys. Lett.* **1994**, *229*, 93.
(25) Miyata, R. M.; Terazima, M. *Anal. Sci.* **2001**, *17*, 231.
(26) Beard, M. C.; Turner, G. M.; Schmuttenmaer, C. A. *J. Am. Chem. Soc.* **2000**, *122*, 11541.
(27) Beard, M. C.; Turner, G. M.; Schmuttenmaer, C. A. *J. Phys. Chem. A* **2002**, *106*, 878.
(28) (a) Zong, Y.; McHale, J. L. *J. Chem. Phys.* **1997**, *106*, 4963. (b) Zong, Y.; McHale, J. L. *J. Chem. Phys.* **1997**, *107*, 2920. (c) Zong, Y.; McHale, J. L. *J. Chem. Phys.* **2004**, *120*, 11333.
(29) McHale, J. L. *Acc. Chem. Res.* **2001**, *34*, 265.
(30) Ishida, T.; Rossky, P. J. *J. Phys. Chem. A* **2001**, *105*, 558.
(31) Zalesny, R.; Bartkowiak, W.; Styrcz, S.; Leszczynski, J. *J. Phys. Chem. A* **2002**, *106*, 4032.
(32) Rao, J. L.; Bhanuprakash, K. *J. Mol. Struct.: THEOCHEM* **1999**, *458*, 269.
(33) Fabian, J.; Rosquete, G. A.; Montero-Cabrera, L. A. *J. Mol. Struct.: THEOCHEM* **1999**, *469*, 163.
(34) Hwang, H.; Rossky, P. J. *J. Phys. Chem. A* **2004**, *108*, 2607.
(35) Frisch, M. J.; Trucks, G. W.; Schlegel, H. B.; Scuseria, G. E.; Robb, M. A.; Cheeseman, J. R.; Montgomery, J. A., Jr.; Vreven, T.; Kudin, K. N.; Burant, J. C.; Millam, J. M.; Iyengar, S. S.; Tomasi, J.; Barone, V.; Mennucci, B.; Cossi, M.; Scalmani, G.; Rega, N.; Petersson, G. A.; Nakatsuji, H.; Hada, M.; Ehara, M.; Toyota, K.; Fukuda, R.; Hasegawa, J.; Ishida, M.; Nakajima, T.; Honda, Y.; Kitao, O.; Nakai, H.; Klene, M.; Li, X.; Knox, J. E.; Hratchian, H. P.; Cross, J. B.; Bakken, V.; Adamo, C.; Jaramillo, J.; Gomperts, R.; Stratmann, R. E.; Yazyev, O.; Austin, A. J.; Cammi, R.; Pomelli, C.; Ochterski, J. W.; Ayala, P. Y.; Morokuma, K.; Voth, G. A.; Salvador, P.; Dannenberg, J. J.; Zakrzewski, V. G.; Dapprich, S.; Daniels, A. D.; Strain, M. C.; Farkas, O.; Malick, D. K.; Rabuck, A. D.; Raghavachari, K.; Foresman, J. B.; Ortiz, J. V.; Cui, Q.; Baboul, A. G.; Clifford, S.; Cioslowski, J.; Stefanov, B. B.; Liu, G.; Liashenko, A.; Piskorz, P.; Komaromi, I.; Martin, R. L.; Fox, D. J.; Keith, T.; Al-Laham, M. A.; Peng, C. Y.; Nanayakkara, A.; Challacombe, M.; Gill, P. M. W.; Johnson, B.; Chen, W.; Wong, M. W.; Gonzalez, C.; Pople, J. A. *Gaussian 03*, revision C.02; Gaussian, Inc.: Wallingford, CT, 2004.
(36) Ahlrichs, R.; Bär, M.; Baron, H.-P.; Bauernschmitt, R.; Böcker, S.; Deglmann, P.; Ehrig, M.; Eichkorn, K.; Elliott, S.; Furche, F.; Haase, F.; Häser, M.; Horn, H.; Hättig, Ch.; Huber, Ch.; Huniar, U.; Kattannek, M.; Köhn, A.; Kölmel, Ch.; Kollwitz, M.; May, K.; Ochsenfeld, Ch.; Öhm, H.; Schäfer, A.; Schneider, U.; Sierka, M.; Treutler, O.; Unterreiner, B.;

von Arnim, M.; Weigend, F.; Weis, P.; Weiss, H. *Turbomole 5.7*; Karlsruhe, Germany, 2004.
(37) Jiminez-Ruis, M.; Gonzales, M. A.; Bermejo, F. J.; Miller, M. A.; Birge, N. O.; Cendoya, I.; Alegria, A. *Phys. Rev. B* **1999**, *59*, 9155.
(38) Le Fevre, R. J. W. *Trans. Faraday Soc.* **1938**, *34*, 1127.
(39) McNeight, S. A.; Smith, C. P. *J. Am. Chem. Soc.* **1936**, *58*, 1718.
(40) Smith, C. P.; Rogers, H. E. *J. Am. Chem. Soc.* **1930**, *52*, 2227.
(41) Smith, C. P.; Stoops, W. N. *J. Am. Chem. Soc.* **1929**, *51*, 3312.
(42) Oh, J.; Kim, C.-S.; Kim, H. K.; Hwang, Y.-H. *Physics A* **2002**, *315*, 308.
(43) Brand, R.; Lunkerheimer, P.; Schneider, U.; Loidl, A. *Phys. Rev. B* **2000**, *62*, 8878.
(44) Miller, M. A.; Jiminez-Ruis, M.; Bermejo, F. J.; Birge, N. O. *Phys. Rev. B* **1998**, *57*, 13977.
(45) Grabowski, Z. R.; Rotkiewicz, K.; Rettig, W. *Chem. Rev.* **2003**, *103*, 3899.
(46) (a) Rettig, W. *Angew. Chem.* **1986**, *98*, 969. (b) Rettig, W. *Angew. Chem., Int. Ed. Engl.* **1986**, *25*, 971.
(47) Kharlanov, V. A.; Abraham, W.; Rettig, W. *J. Photochem. Photobiol., A* **2001**, *142*, 109.
(48) Kasha, M.; Sytnik, A.; Dellinger, B. *Pure Appl. Chem.* **1993**, *65*, 1641.
(49) Knyazhansky, M. I.; Kharlanov, V. A.; Tymyansky, Ya. R. *J. Photochem. Photobiol., A* **1998**, *118*, 151.
(50) Rettig, W.; Kharlanov, V.; Maus, M. *Chem. Phys. Lett.* **2000**, *318*, 173.
(51) (a) Fabian, J.; Zahradnik, R. *Angew. Chem.* **1989**, *101*, 693. (b) Fabian, J.; Zahradnik, R. *Angew. Chem., Int. Ed. Engl.* **1989**, *28*, 677.
(52) Deisenhofer, J.; Epp, O.; Miki, K.; Huber, R.; Michel, H. *J. Mol. Biol.* **1984**, *180*, 385. Deisenhofer, J.; Michel, H. *Science* **1989**, *245*, 1463.
(53) Michl, J.; Bonačić-Koutecký, V. *Electronic Aspects of Organic Photochemistry*; Wiley: New York, 1990.
(54) (a) Bonačić-Koutecký, V.; Koutecký, J.; Michl, J. *Angew. Chem.* **1987**, *99*, 216. (b) Bonačić-Koutecký, V.; Koutecký, J.; Michl, J. *Angew. Chem., Int. Ed. Engl.* **1987**, *26*, 170.
(55) Lippert, E.; Rettig, W.; Bonacic-Koutecky, V.; Heisel, F.; Miehé, J. A. *Adv. Chem. Phys.* **1987**, *1*, 68.
(56) Cogan, S.; Kahan, A.; Zilberg, S.; Haas, Y. *J. Phys. Chem. A* **2008**, *112*, 5604.
(57) Kang, H.; Facchetti, A.; Jiang, H.; Cariati, E.; Righetto, S.; Ugo, R.; Zuccaccia, C.; Macchioni, A.; Stern, Ch. L.; Liu, Z.; Ho, S.-T.; Brown, E. C.; Ratner, M. A.; Marks, T. J. *J. Am. Chem. Soc.* **2007**, *129*, 3267.
(58) Brown, E. C.; Marks, T. J.; Ratner, M. A. *J. Phys. Chem. B* **2008**, *112*, 44.
(59) Stolarczyk, L. Z.; Piela, L. *Chem. Phys.* **1984**, *85*, 451.
(60) Cogan, S.; Kahan, A.; Zilberg, S.; Haas, Y. *J. Phys. Chem. A* **2008**, *112*, 5604.

JP904537K